Demixing effects in mixtures of two bosonic species

F. Lingua, M. Guglielmino, and V. Penna
Department of Applied Science and Technology and u.d.r. CNISM, Politecnico di Torino, I-10129 Torino, Italy

B. Capogrosso Sansone
H. L. Dodge Department of Physics and Astronomy, The University of Oklahoma, Norman, Oklahoma 73019, USA
and Department of Physics, Clark University, Worcester, Massachusetts 01610, USA

(Received 6 August 2015; published 13 November 2015)

Motivated by recent experiments on two-component systems, we investigate the ground-state phase diagram of a mixture of two bosonic species by means of path-integral quantum Monte Carlo simulations by a two-worm algorithm. The mixture is trapped in a square lattice at different filling conditions. Various quantum phases are stabilized depending on the interplay between intra- and interspecies interactions and on the filling factors. We show that the ground-state phase diagram at half-filling features a demixed superfluid phase and a demixed Mott-insulator phase when the interspecies interaction becomes greater than the intraspecies repulsion, and a double-superfluid phase or a supercounterflow otherwise. We show that demixing, characterized by spatial separation of the two species, can be detected experimentally through the effects of anisotropy revealed by time-of-flight images. We also study how demixing effects depend on the filling factor of the two components. Finally, we find that the supercounterflow phase is preserved in the presence of unbalanced populations.

DOI: 10.1103/PhysRevA.92.053610 PACS number(s): 67.85.Fg, 67.60.Bc, 67.85.Hj

I. INTRODUCTION

Mixtures of two bosonic species trapped in optical lattices feature a variety of unprecedented effects and quantum phases [1–25] resulting from the interplay between kinetic energy and intra- and interspecies density-density interactions. In the past decade, considerable theoretical work has been devoted to investigating manifold properties of these systems. Different aspects of the phase diagram have been studied by means of generalized mean-field schemes [15–17], the Luttinger-liquid picture [18], or perturbation methods [19]. Moreover, the effect of phase separation [20,21], the study of quantum emulsions and coherence properties of mixtures [22,23], and the shift of Mott domains due to the presence of a second (superfluid) species [24] along with the interpretation of this shift in terms of polaron excitations [25] have been explored.

In the limit of large interactions, magneticlike phases such as the incompressible double-checkerboard solid and the supercounterflow have been predicted theoretically [1–3] at total filling one and repulsive interspecies interaction, while paired superfluidity has been found [4] in the case of attractive interspecies interaction at equal integer filling of the two components. These findings stimulated further investigation of magneticlike phases including finite-temperature effects [9,13], different optical lattice geometries [14] and dimensionality, and various interacting regimes [5–12,19]. Nevertheless, over 10 years from the initial theoretical investigation of these systems [1–3], their rich phase diagram still exhibits several unexplored aspects that challenge theoretical and numerical techniques, while its elusive character demands more sophisticated experimental techniques for the observation of these quantum phases.

The recent experimental realization of mixtures, either combining two different atomic species [26,27] or using the same atomic species in two different internal energy states [28–31], has demonstrated how refined experimental techniques allow one to control the model parameters, hence reinforcing the interest in these systems. The possibility to observe such new phases in real systems is strongly affected by (i) the presence of the trapping potential which introduces an undesired source of inhomogeneity, (ii) the fact that their theoretic prediction is based on assuming rather ideal conditions (such as, for example, species A and B with the same boson numbers $N_a = N_b$ or large intraspecies interactions), and (iii) the difficulty in reaching low enough temperatures where such phases are expected. Concerning points (i) and (ii), the experimental realizability of magnetic phases has been analyzed in Ref. [32], leading to promising results at least for the double-checkerboard phase. In Ref. [32] it was shown that the double-checkerboard state can be found for large but finite intraspecies interaction and for certain parabolic confinements and particle number imbalance.

In this work, we reconstruct the ground-state phase diagram of a mixture of two twin species (two bosonic components with equal hopping parameters and equal intraspecies interactions) at half-filling $\nu = \frac{1}{2}$ and determine under which conditions the supercounterflow and demixed phases are stabilized. We further explore demixing away from $\nu = \frac{1}{2}$. Demixed phases are characterized by spatial separation of the two species. So far, demixing effects have been mainly studied in the context of continuous systems [33–39] and Bose-Fermi mixtures [40,41]. Here, we study demixing in a binary mixture of bosons described by the two-component Bose-Hubbard model. At $\nu = \frac{1}{2}$ we find a demixed superfluid (dSF) phase or a demixed Mott-insulator (dMI) phase when the interspecies interaction is greater than the intraspecies repulsion, and a double-superfluid (2SF) phase or a supercounterflow (SCF) otherwise. We characterize transitions to demixed phases by introducing a suitable demixing parameter. Further significant information is found by looking at the off-diagonal correlator which allows one to design experimental observation of the various phases through time-of-flight images. We also study SCF away from $\nu = \frac{1}{2}$ and find that SCF is stabilized for

commensurate total filling although the superfluid response in the counterflow channel does depend on the population imbalance. This paper is organized as follows. In Sec. II we present our model and formalism. In Sec. III we discuss the ground-state phase diagram at $\nu = \frac{1}{2}$, supercounterflow properties for unbalanced populations, and the demixing effect at noncommensurate filling. Finally, in Sec. IV we conclude.

II. METHOD AND MODEL

We study a mixture of two bosonic species in a uniform two-dimensional (2D) square optical lattice. The system is described by the two-component Bose-Hubbard (BH) model:

$$H = H_a + H_b + U_{ab} \sum_i n_{ai} n_{bi}, \tag{1}$$

where U_{ab} is the interspecies repulsion, n_{ai} and n_{bi} are the number operators at site i for species A and B, and

$$H_c = \frac{U_c}{2} \sum_i n_{ci}(n_{ci} - 1) - t_c \sum_{\langle ij \rangle} c_i^\dagger c_j, \tag{2}$$

with $c = a,b$ denoting the bosonic species, and operators c_i and $c_i^\dagger$ satisfying the standard commutator $[c_i, c_i^\dagger] = 1$. Parameter U_c represents the intraspecies repulsion and t_c is the hopping amplitude for component c. The symbol $\langle ij \rangle$ refers to summation over nearest neighboring sites. To further simplify the number of free parameters, we work with twin species; that is, we set $U_a = U_b = U$ and $t_a = t_b = t$. We are interested in exploring the phase diagram of model (1) as a function of U/t and U_{ab}/t with particular emphasis on the supercounterflow and demixed phases. Our results are based on large-scale path-integral quantum Monte Carlo simulations by a two-worm algorithm [8,42,43]. Unless otherwise noted, we perform simulations for system sizes $L = 8$, 16, 24, and 36 (we use the lattice step $\lambda/2$ as a unit length) and we work at inverse temperature $\beta = L/t$ which ensures that the system is in its ground state.

III. RESULTS

Ground-state phase diagram at half-filling. The ground-state phase diagram of model (1) is shown in Fig. 1 in the U/t vs U_{ab}/t plane. The 2SF phase features two $U(1)$ broken symmetries and is characterized by order parameters $\langle a \rangle \neq 0$ and $\langle b \rangle \neq 0$, or, equivalently, finite stiffness of the total superfluid flow $\rho_{\rm tot} \neq 0$ and finite stiffness of the relative superfluid flow $\rho_{\rm SCF} \neq 0$. The total and relative superfluid stiffnesses are given by $\rho_{\rm tot,SCF} = \langle (\vec{W}_a \pm \vec{W}_b)^2 \rangle / 2\beta$, where the components of $\vec{W}_a$ and $\vec{W}_b$ are winding numbers of world lines of species A and B [44]. The SCF phase restores one $U(1)$ broken symmetry and is characterized by the order parameter $\langle ab^\dagger \rangle \neq 0$ while $\langle a \rangle = 0$ and $\langle b \rangle = 0$, or, equivalently, zero total superfluid stiffness, $\rho_{\rm tot} = 0$, and finite relative superfluid stiffness, $\rho_{\rm SCF} \neq 0$. The demixed phases are characterized by spatial separation of the two components. This phenomenon is observed whenever $U_{ab} > U$ (as found in Ref. [1] within the isospin picture of bosonic mixtures for the Mott region). A heuristic derivation of this condition for the case of generic filling factor is given in the Appendix. In a demixed phase the density distribution of the two components is anisotropic on the lattice with density maxima of one species corresponding to density minima of the other. The dSF features two $U(1)$ broken symmetries, but the two species occupy different regions of the lattice. Finally, the dMI is an incompressible, insulating phase where the two components are spatially separated. Overall, 2SF and dSF are conducting phases, while dMI and SCF are insulating phases, although SCF supports flow in the so-called particle-hole channel. In agreement with Ref. [45], we find that demixing is observed as soon as $U_{ab}/t > U/t$ for any value of U. It is also worth noting that in order to reach the insulating phases, both intra- and interspecies interactions have to be large enough. Indeed, for $U_{ab}/t \lesssim 13.5$ ($U/t \lesssim 15.5$) the 2SF (dSF) phase is stable for arbitrarily large U/t (U_{ab}/t).

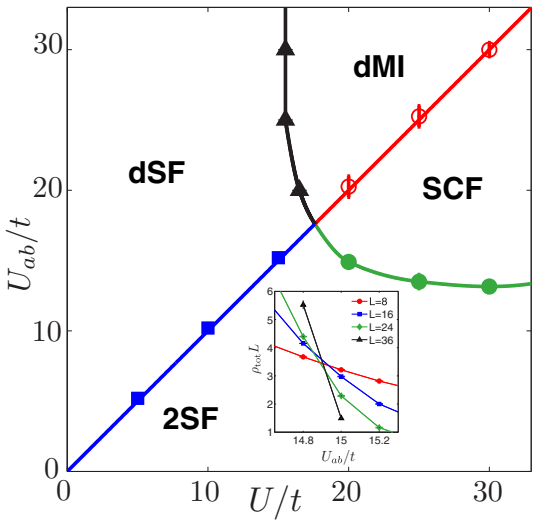

FIG. 1. (Color online) Ground-state phase diagram of twin bosonic species trapped in a uniform optical lattice at $\nu = \frac{1}{2}$. Four phases are stabilized: double superfluid (2SF), supercounterflow (SCF), demixed Mott insulator (dMI), and demixed superfluid (dSF). Symbols mark the phase boundaries as calculated from Monte Carlo simulations (see text). Whenever not visible, error bars lie within the symbol size. The inset shows the scaled total superfluidity $\rho_{\rm tot}$ as a function of the interspecies interaction for system sizes $L = 8$, 16, 24, and 36 and $U/t = 20$. The intersection between curves corresponding to different system sizes gives the transition point for the 2SF-SCF transition.

In order to extract the phase diagram shown in Fig. 1 we measure superfluid stiffness in terms of winding numbers statistics and the demixing parameter Δ (see below) which depends on the density distribution. Both observables are readily available within the path-integral formulation by the worm algorithm. The demixing parameter is given by

$$\Delta = \frac{1}{M} \sum_i \left[\frac{\langle n_{ai} \rangle - \langle n_{bi} \rangle}{\langle n_{ai} \rangle + \langle n_{bi} \rangle} \right]^2, \tag{3}$$

where $\langle n_{ci} \rangle$ is the quantum-thermal average of the density of component $c = a,b$ at site i. Parameter (3) is basically a lattice average of the square of the imbalance of the local species' density. This parameter is different than the one used in Ref. [33], $D = \left[\frac{\langle N_a \rangle - \langle N_b \rangle}{\langle N_a \rangle + \langle N_b \rangle} \right]^2$, but gives the same information about demixed phases.

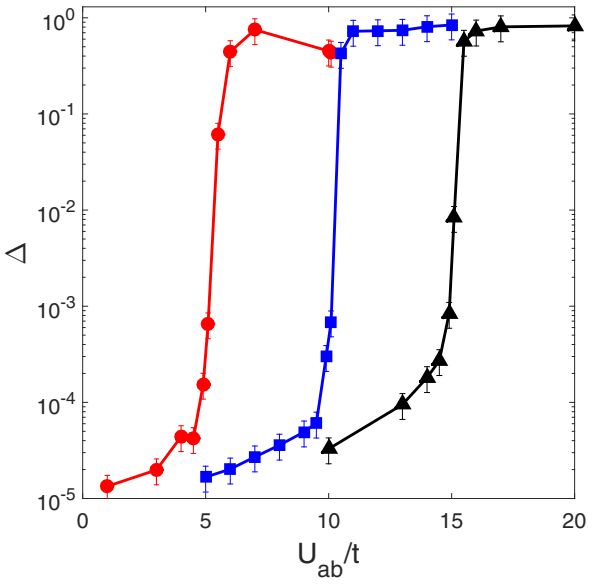

FIG. 2. (Color online) Demixing parameter Δ as a function of U_{ab}/t for $U/t = 5$, 10, and 15 (circles, squares, and triangles, respectively) across the 2SF-dSF transition. A jump of 4 orders of magnitude is clearly visible when $U_{ab}/t \sim U/t$, signaling the onset of the demixed phase dSF at the expense of the 2SF phase.

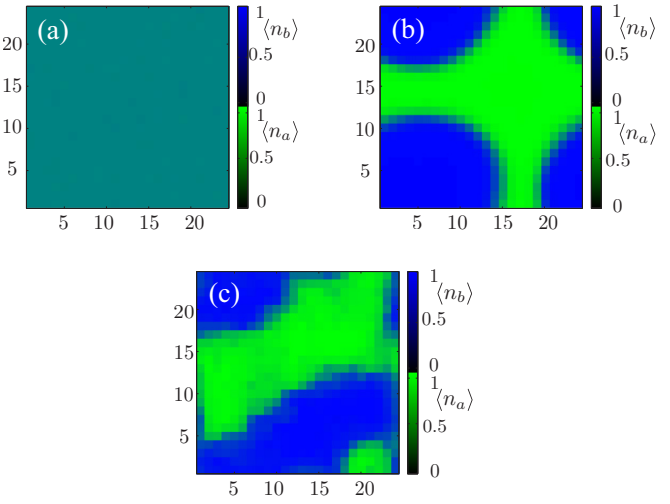

FIG. 3. (Color online) Quantum-statistical average of the particle numbers $\langle n_{ai} \rangle$ and $\langle n_{bi} \rangle$. The x and y axes denote the x and y coordinates on the lattice. The color code is displayed in the the bar on the right-hand side. (a) 2SF phase at $U/t = 10$ and $U_{ab}/t = 7$ with density uniformly distributed in the lattice. (b) dSF phase at $U/t = 15$ and $U_{ab}/t = 20$ with two components occupying spatially separated regions of the lattice. (c) dMI phase at $U/t = 20$ and $U_{ab}/t = 22$ with two components occupying spatially separated regions of the lattice. Compenetration between the two regions is noticeable.

In Fig. 1, solid circles correspond to the 2SF-SCF transition. This transition belongs to the (2+1)-XY universality class. Transition points are found using standard finite-size scaling of ρ_{tot} as can be seen in the inset of Fig. 1 where we plot the scaled total superfluidity as a function of interaction U_{ab}/t for system sizes $L = 8$, 16, 24, and 36 and $U/t = 20$. The curves corresponding to different sizes intersect at the critical point $U_{ab}/t = 14.9 \pm 0.1$. Both 2SF and SCF are stable for $U_{ab} < U$.

We detect the phase transition between 2SF and dSF (squares in Fig. 1) by studying the behavior of the Δ parameter. In Fig. 2 we show Δ as a function of U_{ab}/t for $U/t = 5$, $U/t = 10$, and $U/t = 15$, circles, squares, and triangles, respectively. A jump of 4 orders of magnitude is clearly visible when $U_{ab}/t \sim U/t$, signaling the onset of the demixed phase dSF at the expense of the 2SF phase. Further significant information about the demixed phase is achieved by looking at the density distribution of particles in the lattice. The quantum-statistical average of the particle numbers $\langle n_{ai} \rangle$ and $\langle n_{bi} \rangle$ is displayed in Fig. 3. The x and y axes denote the x and y coordinates on the lattice. The color code is displayed in the bar on the right-hand side. Figure 3(a) refers to the 2SF case where the density of each species is uniformly distributed in the lattice, corresponding to the spatial coexistence of the two species. Figure 3(b) refers to the dSF phase. Here, we clearly see that the two components occupy spatially separated regions with well-defined boundaries of a few lattice steps of thickness where the two components coexist.

The dSF phase becomes unstable towards a dMI phase upon increasing the intraspecies interaction (triangles in Fig. 1). We compute the phase boundary by verifying the drop of the SF density of each component for system sizes $L = 8$, 16, and 24. While the dSF is characterized by two $U(1)$ broken symmetries over spatially separated regions, in the dMI phase these symmetries are restored; that is, the system loses its off-diagonal long-range (anisotropic) correlations and becomes insulating. Investigating the details of this phase transition is challenging. Finite-size scaling of the SF stiffness cannot be performed in proximity of demixed regions since the statistics of winding numbers is affected by the topography and the (nonconnected vs connected) topology of demixed regions, both of which depend on the initial conditions. The averaged particle number within the lattice in the dMI phase is displayed in Fig. 3(c) . Unlike the dSF phase [Fig. 3(b)], the boundaries between the regions occupied by the two species tend to be rough and irregular, and compenetration between the regions is more pronounced due to the reduced mobility of bosons in the dMI phase.

Finally the empty circles in Fig. 1 correspond to the SCF-dMI transition. Upon entering the dMI the system restores the $U(1)$ broken symmetry characterizing the SCF. We measured the Δ parameter and ρ_{SCF} across the transition line and, similarly to the 2SF-dSF transition, we observe an increase of about 3 orders of magnitude in Δ, while ρ_{SCF} goes to 0.

In Fig. 4 we show the computed momentum distributions $n_{c\mathbf{k}} = |\phi_{(\mathbf{k})}|^2 \sum_{i,j} e^{i\mathbf{k}(\mathbf{r}_i - \mathbf{r}_j)} \langle c_i^\dagger c_j \rangle$ [46] for species $c = a, b$ proportional to time-of-flight (TOF) images detectable experimentally. Here $\phi_{(\mathbf{k})}$ is the Fourier transform of the Wannier function $\phi(\mathbf{r})$, which we do not compute here. TOF profiles along x and y lattice directions within the first Brillouin zone are plotted in Fig. 4 for the 2SF [panel (a)], dSF [panel (b)], SCF [panel (c)], and dMI [panel (d)] phases. Note that the TOF image of the SCF phase corresponds to the one of the particle-hole pair. The insets show the corresponding quantum-statistical average of the density of

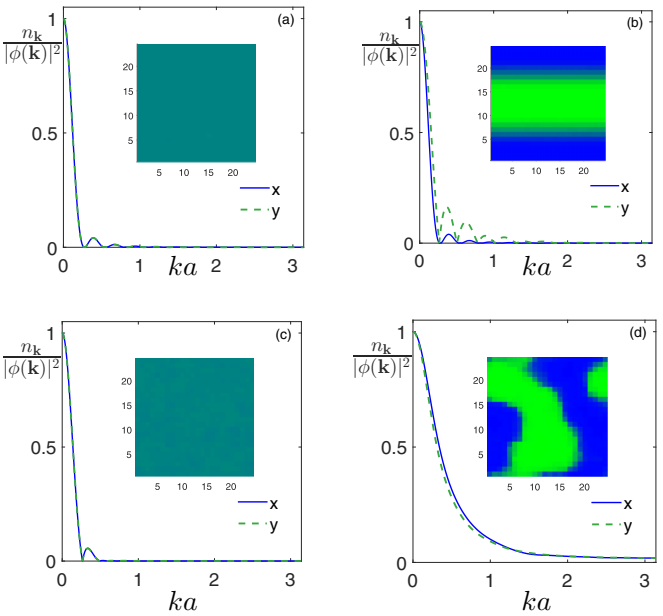

FIG. 4. (Color online) Momentum distributions n_k in the first Brillouin zone for the 2SF (a), dSF (b), SCF (c), and dMI (d)] phases. The insets show the corresponding quantum-statistical average of the density of the two components within the lattice. The dSF phase shows an evident anisotropy along the x and y directions. This is expected due to the anisotropy of the spatial separation.

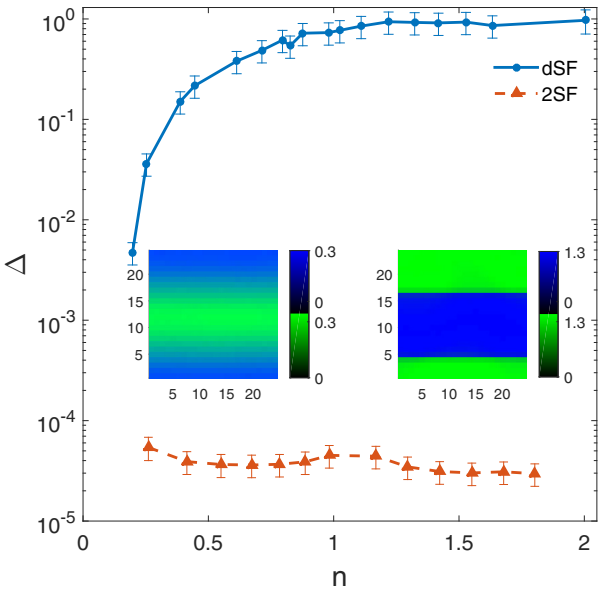

FIG. 5. (Color online) Δ parameter as a function of total filling n for the dSF (circles, $U/t = 10$, $U_{ab}/t = 15$, and $L = 24$) and 2SF (triangles, $U/t = 10$, $U_{ab}/t = 7$, and $L = 24$) phases. Insets represent the average densities of the two components for $n = 0.3$ (left) and $n = 1.3$ (right).

the two components within the lattice. We observe different profiles featuring the different quantum phases with an evident detectable anisotropy of distributions $n_{c\mathbf{k}}$ along the x and y directions for dSF phase. This is expected due to the anisotropy of the spatial separation and represents a clear experimental signature of the dSF phase. On the other hand the TOF image of the dMI phase doesn't reflect anisotropy of spatial separation due to the absence of off-diagonal long-range order. In general, we observe no differences in the momentum distributions between the two species.

Noncommensurate filling. We now turn to studying model (1) away from commensurate total filling where neither the dMI phase nor the SCF phase exists. In particular, we are interested in studying the properties of the dSF phase as a function of the total filling n. We find that demixing effects are still present at $n < 1$, although the spatial separation between the two components A and B is not as pronounced as for $n \geqslant 1$. This can be seen in Fig. 5, where we plot the demixing parameter Δ as a function of n (circles). A substantial drop in the value of Δ is observed for $n < 1$. This is due to the presence of large regions in the lattice where A and B overlap, as shown in the left inset of Fig. 5 where we plot the quantum-statistical average of the densities of the two species at $n = 0.3$. This overlap region results from enhanced hopping of particles which is responsible for larger fluctuations of $\langle n_{a,b} \rangle$. For comparison, in the right inset of Fig. 5, we show the species densities at $n = 1.3$. A net spacial separation between A and B is observed. Despite this substantial drop in the value of Δ for $n < 1$, we find that Δ is still a good indicator that demixing has occurred. Indeed, Δ values in the 2SF phase (triangles in Fig. 5) are still orders of magnitude smaller than those in the dSF phase. These results suggests that demixing effects can be observed in the presence of an external harmonic trap where a variation of n within the trap is present. See Supplemental Material [47] for further details.

Unbalanced populations. We conclude by studying the SCF phase in the presence of population imbalance. The SCF phase can be stabilized at $n = 1$. Here we are interested in showing that the SCF phase still exists with nonzero imbalance although its robustness depends on the latter. In Fig. 6 we plot ρ_{SCF} for different values of the ratio N_b/N_a. We observe that the SCF phase remains robust also for large population imbalance although the largest superfluid response corresponds to the balanced case.

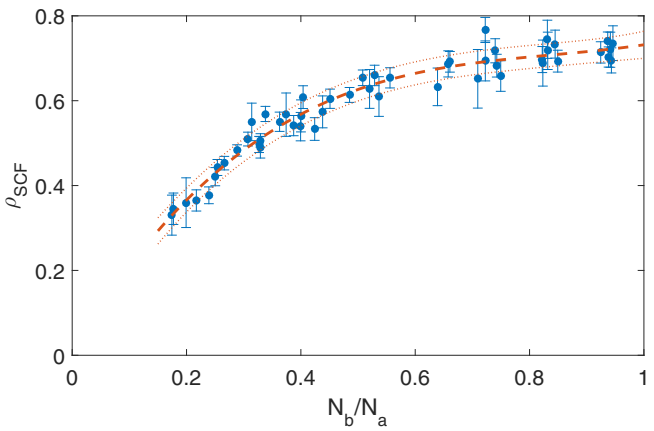

FIG. 6. (Color online) Supercounterfluidity stiffness as a function of N_b/N_a ($U/t = 20$, $U_{ab}/t = 17$, and $L = 24$). The dashed line is a cubic polynomial least-square fit, while the dotted lines represent 1-σ deviation contours from the fit.

IV. CONCLUSION

Motivated by recent experiments on two-component systems, we investigated properties of a mixture trapped in a 2D optical lattice at different filling factors. We used path-integral quantum Monte Carlo simulations by a two-worm algorithm. At $\nu = \frac{1}{2}$, we observed a dSF phase and a dMI phase when the interspecies interaction becomes greater than the intraspecies repulsion, and a dSF phase or a SCF phase otherwise. Demixing was characterized by spatial separation of the two components and manifested itself experimentally with anisotropic TOF images. The latter were calculated for selected examples, comparing the results for demixed and non-demixed phases. Finally, we showed that the SCF phase survives in the presence of population imbalance and trapping potential (see Supplemental Material [47]). In the future, we plan to investigate how finite temperature affects demixing. Our preliminary results show that, in the dSF phase, thermal fluctuations destroy demixing effects earlier than they destroy superfluidity, leaving the system in a uniform superfluid phase. Moreover, since preliminary results show that the demixing parameter is sensitive to temperature, this suggests its possible application as a thermometer for mixtures of ultracold gases.

ACKNOWLEDGMENTS

We thank F. Minardi for fruitful discussions. This work was supported by MIUR (PRIN 2010LLKJBX) and by the NSF (Grant No. PIF-1415561). The computing for this project was performed at the OU Supercomputing Center for Education and Research (OSCER) at the University of Oklahoma (OU).

APPENDIX: A SIMPLE INTERPRETATION OF THE DEMIXING EFFECT

The mixing-demixing effect can be interpreted in a simple way for the dSF-SF transition at generic filling factor. In a perturbative framework, where the energy contribution of tunneling processes is assumed to be negligible, one should compare the energy of the ground state with the two species spatially separated to the energy of the ground state where the two species coexist within the lattice. When the two species occupy spatially separated regions of the lattice, $\mathcal{R}_a$ and $\mathcal{R}_b$, we assume that M_a (M_b) sites of $\mathcal{R}_a$ ($\mathcal{R}_b$) are occupied by bosons A (B), with r_a (r_b) sites containing $n+1$ ($m+1$) bosons and $M_a - r_a$ ($M_b - r_b$) sites containing n (m) bosons. Note that the total number of sites is given by $M = M_a + M_b$ while the total numbers of particles are $N_a = M_a n + r_a$ and $N_b = M_b m + r_b$. The nonuniform filling in $\mathcal{R}_a$ and $\mathcal{R}_b$ reflects the SF character of the two species. The resulting energy reads

$$E_0 = \frac{U_a}{2} M_a n(n-1) + \frac{U_b}{2} M_b m(m-1) + U_a r_a n + U_b r_b m - \mu_a N_a - \mu_b N_b, \quad \text{(A1)}$$

where the U_{ab}-dependent term is absent due to the spatial separation of the two species. The mixing effect is described by the following: a boson is lost from each site of $\mathcal{R}_a$ ($\mathcal{R}_b$) occupied by $n+1$ ($m+1$) bosons while r_a (r_b) sites appear in $\mathcal{R}_b$ ($\mathcal{R}_a$) with m bosons B and one boson A (n bosons A and one boson B). The U_{ab} interaction term is now activated and the resulting energy is

$$E_0' = \frac{U_a}{2} M_a n(n-1) + \frac{U_b}{2} M_b m(m-1) + U_{ab}(r_a m + r_b n) - \mu_a N_a - \mu_b N_b. \quad \text{(A2)}$$

This mutual exchange of bosons between $\mathcal{R}_a$ and $\mathcal{R}_b$ represents the mixing process with the lowest-energy cost in the minimum-energy scenario. The condition $E_0 < E_0'$ (justifying the transition from the uniform ground state to the demixed state) implies that $U_{ab}(r_a m + r_b n) > U_a r_a n + U_b r_b m$, which reduces to the well-known condition $U_{ab} > U$ for $n = m$ and $U_a = U_b$. This elementary argument is valid in the SF regime due to its semiclassical character. It cannot be extended to the transition from the dMI phase to the SCF phase where quantum correlations and hopping processes play a prominent role.

[1] A. B. Kuklov and B. V. Svistunov, Phys. Rev. Lett. **90**, 100401 (2003).
[2] L.-M. Duan, E. Demler, and M. D. Lukin, Phys. Rev. Lett. **91**, 090402 (2003).
[3] E. Altman, W. Hofstetter, E. Demler, and M. D. Lukin, New J. Phys. **5**, 113 (2003).
[4] A. B. Kuklov, N. Prokof'ev, and B. V. Svistunov, Phys. Rev. Lett. **92**, 050402 (2004).
[5] A. Argüelles and L. Santos, Phys. Rev. A **75**, 053613 (2007).
[6] A. Hu, L. Mathey, I. Danshita, E. Tiesinga, C. J. Williams, and C. W. Clark, Phys. Rev. A **80**, 023619 (2009).
[7] A. Hubener, M. Snoek, and W. Hofstetter, Phys. Rev. B **80**, 245109 (2009).
[8] S. G. Söyler, B. Capogrosso-Sansone, N. V. Prokof'ev, and B. V. Svistunov, New J. Phys. **11**, 073036 (2009).
[9] B. Capogrosso-Sansone, S. G. Söyler, N. V. Prokof'ev, and B. V. Svistunov, Phys. Rev. A **81**, 053622 (2010).
[10] T. Ohgoe and N. Kawashima, Phys. Rev. A **83**, 023622 (2011).
[11] C.-M. Chung, S. Fang, and P. Chen, Phys. Rev. B **85**, 214513 (2012).
[12] Y. Li, L. He, and W. Hofstetter, New J. Phys. **15**, 093028 (2013).
[13] Y. Nakano, T. Ishima, N. Kobayashi, T. Yamamoto, I. Ichinose, and T. Matsui, Phys. Rev. A **85**, 023617 (2012).
[14] J.-P. Lv, Q.-H. Chen, and Y. Deng, Phys. Rev. A **89**, 013628 (2014).
[15] A. Isacsson, Min-Chul Cha, K. Sengupta, and S. M. Girvin, Phys. Rev. B **72**, 184507 (2005).
[16] M. Guglielmino, V. Penna, and B. Capogrosso-Sansone, Laser Phys. **21**, 1443 (2011).
[17] R. V. Pai, J. M. Kurdestany, K. Sheshadri, and R. Pandit, Phys. Rev. B **85**, 214524 (2012).
[18] L. Mathey, Phys. Rev. B **75**, 144510 (2007).
[19] M. Iskin, Phys. Rev. A **82**, 033630 (2010).

[20] T. Mishra, R. V. Pai, and B. P. Das, Phys. Rev. A **76**, 013604 (2007).
[21] P. Jain and M. Boninsegni, Phys. Rev. A **83**, 023602 (2011).
[22] T. Roscilde and J. I. Cirac, Phys. Rev. Lett. **98**, 190402 (2007).
[23] P. Buonsante, S. M. Giampaolo, F. Illuminati, V. Penna, and A. Vezzani, Phys. Rev. Lett. **100**, 240402 (2008).
[24] M. Guglielmino, V. Penna, and B. Capogrosso-Sansone, Phys. Rev. A **82**, 021601(R) (2010).
[25] D. Benjamin and E. Demler, Phys. Rev. A **89**, 033615 (2014).
[26] J. Catani, L. De Sarlo, G. Barontini, F. Minardi, and M. Inguscio, Phys. Rev. A **77**, 011603(R) (2008).
[27] G. Thalhammer, G. Barontini, L. De Sarlo, J. Catani, F. Minardi, and M. Inguscio, Phys. Rev. Lett. **100**, 210402 (2008).
[28] B. Gadway, D. Pertot, R. Reimann, and D. Schneble, Phys. Rev. Lett. **105**, 045303 (2010).
[29] B. Gadway, D. Pertot, J. Reeves, and D. Schneble, Nat. Phys. **8**, 544 (2012).
[30] P. Soltan-Panahi, J. Struck, P. Hauke, A. Bick, W. Plenkers, G. Meineke, C. Becker, P. Windpassinger, M. Lewenstein, and K. Sengstock, Nat. Phys. **7**, 434 (2011).
[31] P. Soltan-Panahi, D. S. Luhmann, J. Struck, P. Windpassinger, and K. Sengstock, Nat. Phys. **8**, 71 (2012).
[32] M. Guglielmino, V. Penna, and B. Capogrosso-Sansone, Phys. Rev. A **84**, 031603(R) (2011).
[33] P. Jain, S. Moroni, M. Boninsegni, and L. Pollet, Phys. Rev. A **88**, 033628 (2013).
[34] Y. Eto, M. Kunimi, H. Tokita, H. Saito, and T. Hirano, Phys. Rev. A **92**, 013611 (2015).
[35] S. Tojo, Y. Taguchi, Y. Masuyama, T. Hayashi, H. Saito, and T. Hirano, Phys. Rev. A **82**, 033609 (2010).
[36] S. B. Papp, J. M. Pino, and C. E. Wieman, Phys. Rev. Lett. **101**, 040402 (2008).
[37] E. Nicklas, H. Strobel, T. Zibold, C. Gross, B. A. Malomed, P. G. Kevrekidis, and M. K. Oberthaler, Phys. Rev. Lett. **107**, 193001 (2011).
[38] E. Nicklas, W. Muessel, H. Strobel, P. G. Kevrekidis, and M. K. Oberthaler, arXiv:1407.8049.
[39] P. Ao and S. T. Chui, Phys. Rev. A **58**, 4836 (1998).
[40] L. Pollet, M. Troyer, K. Van Houcke, and S. M. A. Rombouts, Phys. Rev. Lett. **96**, 190402 (2006).
[41] L. Pollet, C. Kollath, U. Schollwock, and M. Troyer, Phys. Rev. A **77**, 023608 (2008).
[42] N. V. Prokof'ev, B. V. Svistunov, and I. S. Tupitsyn, Phys. Lett. A **238**, 253 (1998).
[43] N. V. Prokof'ev, B. V. Svistunov, and I. S. Tupitsyn, Sov. Phys. JETP **87**, 310 (1998).
[44] E. L. Pollock and D. M. Ceperley, Phys. Rev. B **36**, 8343 (1987).
[45] F. Zhan and I. P. McCulloch, Phys. Rev. A **89**, 057601 (2014).
[46] V. A. Kashurnikov, N. V. Prokof'ev, and B. V. Svistunov, Phys. Rev. A **66**, 031601 (2002).
[47] See Supplemental Material at http://link.aps.org/supplemental/10.1103/PhysRevA.92.053610 for the investigation of the effects of the trapping potential and of different fillings on the dSF and SCF phases.